Siberian Branch of Russian Academy of Science
BUDKER INSTITUTE OF NUCLEAR PHYSICS

V.N. Baier and V.M. Strakhovenko

COMPARISON OF THEORY WITH EXPERIMENT FOR POSITRON PRODUCTION FROM HIGH-ENERGY ELECTRONS MOVING ALONG CRYSTAL AXES

Budker INP 2002-14

Novosibirsk
2002

Comparison of theory with experiment for positron production from high-energy electrons moving along crystal axes

V.N. Baier and V.M. Strakhovenko

Budker Institute of Nuclear Physics
630090 Novosibirsk, RF

Abstract

Various positron distributions are obtained using an approach developed earlier for the description of the electron - photon showers in axially aligned single crystals. Based on these distributions, characteristics of the positron yield measured in recent experiments are calculated. Theoretical estimations display a rather good agreement with experimental results obtained using 3 to 10 GeV electrons aligned to the $< 111 >$-axis of the tungsten crystals.

1 Introduction

An efficient positron source is one of the important components of future electron-positron colliders. Positrons are generated from electrons in the course of the $e^-e^+\gamma$-shower developing in a medium. In high-energy region, the basic processes involved in the shower development are typically considerably enhanced in oriented crystals as compared with corresponding amorphous media . The most pronounced effects take place at axial alignment when initial electrons are moving along the main axes of a crystal. This alignment alone will be considered below. Then, according to [1],the radiation intensity in a crystal exceeds that of the conventional bremsstrahlung starting with electron energies $\varepsilon \sim 1$ GeV. Simple estimations of the width of the power spectrum performed in [1] indicate a soft character of this spectrum. Basing on these properties of the photon emission process, the use of this phenomenon in positron source for future accelerators was proposed [2]. The pair production rate which is due to the coherent (crystal) effects exceeds that of the standard (Bethe-Heitler) mechanism starting with photon energies $\omega \simeq \omega_{th}$. The value of ω_{th} is about 22 GeV for the $< 111 >$-axis of tungsten being several times larger for another crystals. (See review [3] and recent book [4] for further details concerning QED-processes in crystals.) For energies well above ω_{th}, the crystal effects become really strong and may be used to create effective and compact electromagnetic calorimeters [5]. For very high energies ($\varepsilon \gg \omega_{th}$) of initial and created particles, kinetic equations describing the shower development were solved analytically [6]. Though the initial electron energies were high enough in the first experimental investigation [7] of shower formation in crystals, energies of detected particles were too low to allow us the direct comparison with [6]. To explain the results of [7], Monte-Carlo simulations were performed in [8]. The probabilities of basic processes used in [8] were obtained within so-called constant field approximation. A good agreement was demonstrated in [8] with the results of [7] for Ge crystals.

When the initial electron energy is below ω_{th}, photons are mainly emitted with energies $\omega \ll \omega_{th}$ and so, up to minor modifications (see [9], [10]), the pair production process proceeds in a crystal as in an amorphous medium. The enhancement of radiation from initial electrons is thereby the main crystal effect in this energy region. A substantial advance in the description of shower formation at axial alignment was caused by the invention of the semiphenomenological radiation spectrum [11] . This allows one to consider the relatively low (of a few GeV) energy range of the initial electrons which is presumed for the efficient positron source. The radiation intensity increases with the initial electron energy. As a result, at some energy the effective radiation length L_{ef} in a crystal becomes smaller than the conventional radiation length L_{rad} and continues its decrease at further increase of the energy. All numerical examples will be given below for the electron beam aligned with the $< 111 >$-axis of the tungsten crystals. Then we have for the quantity L_{ef} defined as in Sec.3 of [11]: $L_{ef}(1\ \mathrm{Gev}) \simeq 0.166$ cm, $L_{ef}(4\ \mathrm{Gev}) \simeq 0.084$ cm, and $L_{ef}(8\ \mathrm{Gev}) \simeq 0.061$ cm. In a hybrid target which consists of the crystal part followed by the amorphous one, a thickness of the crystal constituent of several L_{ef} is obviously quite enough. Indeed, at the depth $L_0 \approx (3 \div 4)L_{ef}$ most of the particles, including the initial electrons, are sufficiently soft to reduce the coherent contribution to the radiation to the level of the incoherent one. Thereby, the further development of the shower proceeds more or less in the same way for the crystal or amorphous type of the remaining part of a target. We emphasize that the crystal part $L \leq L_0$ of a target serves as a radiator, and secondary charged particles are still not so numerous at this stage of the shower development. Therefore only a small portion of the total energy loss is deposited in the crystal part of a target which considerably reduces a danger of its overheating. The softness of photon spectra is another important feature of the crystal radiator giving additional advantages for the positron production in comparison with the entirely amorphous target. To get more definite idea concerning a shape of the power spectrum one can use its explicit form given by Eq.(2) in [11]. To present the scale, let us list some values ω_{max} where this spectrum is maximum: $\omega_{max}(1\ \mathrm{GeV}) \simeq 31$ MeV, $\omega_{max}(4\ \mathrm{GeV}) \simeq 170$ MeV, and $\omega_{max}(8\ \mathrm{GeV}) \simeq 490$ MeV. Note that a width of the spectrum is typically several times larger than ω_{max}. The increase in the number of relatively soft photons turns out to be much more pronounced than that in the total radiation intensity. In the end, just this fact leads to the substantial enhancement of the positron yield from crystal targets.

Recently the positron production in axially aligned single crystals was studied in two series of experiments performed at CERN [12], [13] and KEK [14], [15]. The initial energy of electrons was 3 GeV [14], 6 and 10 GeV

[13], 8 GeV [15], and 10 GeV [12]. In all cases the initial electron beam was aligned with the $<111>$-axis of a tungsten crystal that sometimes served as the crystal part of a hybrid target which contained an additional amorphous tungsten target. A noticeable enhancement of the low-energy positron yield was observed in all experiments cited above when the yield from a crystal target was compared with that from an amorphous target of the same thickness. The experimental results and our theoretical estimations presented in the next Section display a rather good agreement with each other.

2 Comparison of theory with experiment

Theoretical results for the conditions of the experiments cited above were obtained using the approach developed in [11] and [10] where various positron and photon distributions as well as deposited energies in different crystals were calculated for the energy range of initial electrons from 2 to 300 GeV. In these papers, all the formulas used in Monte-Carlo simulations of the specific $e^-e^+\gamma$-shower characteristics are given in the explicit form. Remember that our simplified description of the shower development takes into account coherent (induced by the regular motion of particles in the field of crystal axes) and incoherent (like that in an amorphous medium) mechanisms of photon emission and pair production processes. The multiple scattering and the ionization energy loss of electrons and positrons are taken into account neglecting crystal effects. The coherent radiation from channelling and moving not very high above the axis potential barrier particles is described using the semi-phenomenological spectrum suggested in [11]. A corresponding computer code was developed. This allows one to calculate energy, angular, and coordinate distributions of positrons emergent from a crystal or hybrid target and to find an amount of the energy deposition. We think that the investigation of such distributions should be the main object of the experiments having a creation of the crystal assisted positron source as their ultimate aim.

2.1 Experiment (CERN) at $\varepsilon_0 = 10$ GeV

Among experiments cited above, spectral-angular distributions of created positrons were measured only in WA103 experiment at CERN (see [12], [13]) where our code was used in simulations as the event generator. This simulation allowed for the acceptance conditions and the efficiency of the detectors used. Shown in Fig.1 taken from [13] is one example of the measured and

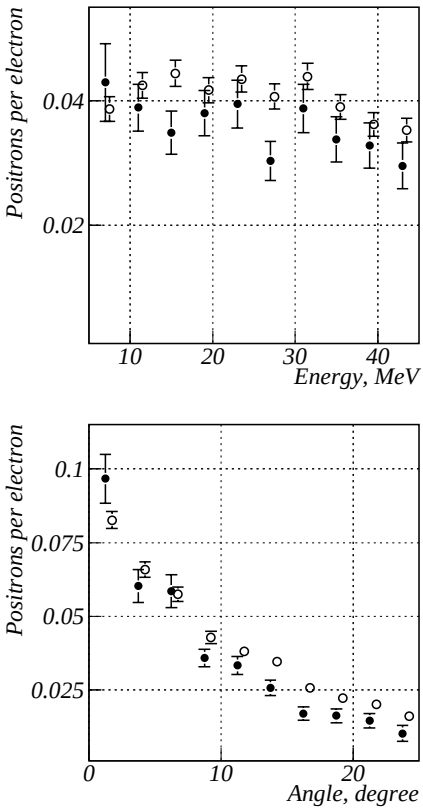

Figure 1: Spectral (left) and angular (right) distributions of positrons from 10 GeV electrons traversing 8-mm-thick crystal tungsten target along the $< 111 >$-axis. Open circles - simulation, filled circles - experiment.

simulated distributions of positrons from 10-GeV electrons aligned with the $< 111 >$-axis of the 8-mm-thick crystal tungsten. The angular acceptance conditions in WA103 experiment were approximately $|\vartheta_V^{out}| \leq 1.5^\circ$ for the vertical and $0 \leq \vartheta_H^{out} \leq 25^\circ$ for the horizontal angle of outgoing positron with respect to the initial electron beam direction. We shell see below that a shape of the positron spectrum depends on a degree of collimation. The one-dimensional (over ϑ_H^{out}) angular distribution is presented for positrons having energies in the 5÷45 MeV range. We emphasize that a relative difference between measured and simulated results typically does not exceed 20% in both spectral and angular distributions as seen in Fig.1. We are aware that

preliminary results for another settings used in the same experiment do not contradict with the estimated scale of the difference between the data and theoretical predictions. We hope that this interrelation will not become worse after performing the complete analysis of the data which now is underway. This analysis will also give more detailed information concerning spectral-angular distributions of positrons depending on initial electron energies and target thicknesses.

2.2 Experiment (KEK) at $\varepsilon_0 = 3$ GeV

The main goal of the experiment [14] was an attempt to apply the crystal target to a working electron/positron linac, the injector for the electron-positron collider B-Factory at KEK. Thus, the acceptance conditions for created positrons were determined by the momentum acceptance of the positron linac with a matching section which is $8.2 < p < 11.6$ MeV/c and $p_\perp < 2.4$ MeV/c. The hybrid target used consists of 1.7-mm-thick tungsten crystal followed by 7-mm-thick amorphous tungsten. The observed positron yield was enhanced by the factor 1.40 when the $< 111 >$-crystal axis was aligned with 3 GeV incident electron beam as compared to the case of the disoriented crystal. Our number for this enhancement is 1.47 being only 5% larger than the experimental one. Note that in the experiment [14] the crystal and amorphous parts of the hybrid target were separated by the distance of 70 mm. This circumstance, which, in principle, may slightly change the enhancement value, was not taken into account in our calculation. Recollect that an amount of the energy deposited in the crystal part (ε_{dep}^{cr}) of a hybrid target may be much smaller than that (ε_{dep}^{am}) in the amorphous one. Such interrelation of ε_{dep}^{cr} and ε_{dep}^{am} should take place in the case of [14], where the crystal thickness is about 1.8 L_{ef} (see discussion in the Introduction). This is confirmed by our calculations which give $\varepsilon_{dep}^{cr} \simeq 11$ MeV and $\varepsilon_{dep}^{am} \simeq 277$ MeV per one incident electron.

2.3 Qualitative features of positron distributions and experiment (KEK) at $\varepsilon_0 = 8$ GeV

In [15] the positron production efficiency from 2.2, 5.3 and 9.0-mm-thick tungsten crystals was measured using an 8-GeV electron beam. Positrons produced in the forward direction with momenta 10, 15 and 20 MeV/c were detected by a magnetic spectrometer. Thus, only several points in the energy distribution were determined under hard collimation conditions. Therefore, before going on to the comparison of the experimental results with our, let us

remind some important qualitative features of spectral-angular distributions using 8 GeV electrons and the $<111>$-axis of the tungsten crystals as an example. For the sake of comparison, the corresponding distributions for amorphous tungsten will be presented as well. Below all the quantities characterizing a positron yield are normalized per one incident electron.

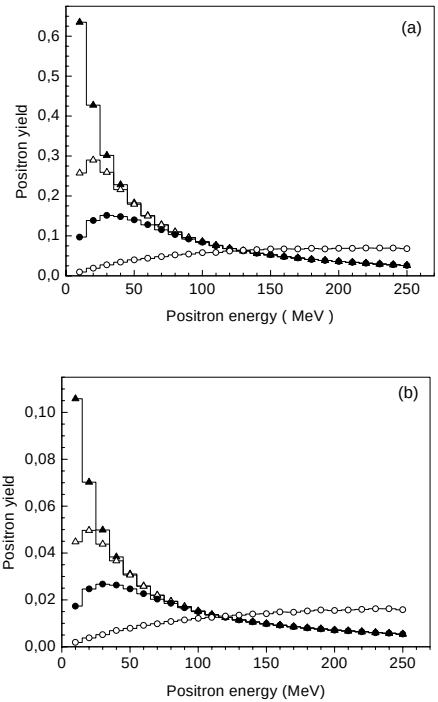

Figure 2: Positron yield depending on energy from 2.2-mm-thick crystal (a) and amorphous (b) targets at different collimation. Filled triangles - no collimation ($\vartheta_{out} \leq 180°$), open triangles - $\vartheta_{out} \leq 24°$, filled circles - $\vartheta_{out} \leq 12°$, and open circles - $\vartheta_{out} \leq 1°$ (multiplied by 10).

The use of matching systems implies some collimation (typically $\vartheta_{out} \leq 25°$) of outgoing positrons. Shown in Fig.2 is the energy dependence (energy step is equal to 10 MeV) of the positron yield from crystal (a) and amorphous (b) targets of the same thickness $L = 2.2$ mm. In the case of the hard collimation, when $\vartheta_{out} \leq 1°$ (open circles), the yield is multiplied by 10 to make it visible. The larger a positron energy, the

smaller is a typical value of ϑ_{out} since both production and multiple scattering processes are characterized by smaller angles for higher energies. This is seen in Fig.2 (a) where non-collimated spectrum joins that for $\vartheta_{out} \leq 24^\circ$ at $\varepsilon_{cr}^{(1)} \simeq 55$ MeV. The latter, in turn, joins the spectrum for $\vartheta_{out} \leq 12^\circ$ at $\varepsilon_{cr}^{(2)} \simeq 110$ MeV. Such behavior is also seen in Fig.2 (b) for the amorphous target where $\varepsilon_{am}^{(1)} \simeq 50$ MeV and $\varepsilon_{am}^{(2)} \simeq 105$ MeV. In other words, positrons with energies $\varepsilon > \varepsilon^{(1)}$ are practically concentrated within a cone $\vartheta_{out} \leq 24^\circ$ and those with $\varepsilon > \varepsilon^{(2)}$ have $\vartheta_{out} \leq 12^\circ$. In accordance with this picture, the spectral maximum is shifted to the right while a width of the distribution increases when the collimation angle decreases. The enhancement μ, being bin-by-bin ratio of the positron yield from a crystal target to that from an amorphous one at the same collimation, is almost constant for $\varepsilon < 45$ MeV and monotonically decreases with growing positron energy. This means that positron spectra from a crystal target are softer. Somewhat lower values of $\varepsilon^{(1)}, \varepsilon^{(2)}$ in the amorphous case point at the same feature. For given collimation, a variation of the enhancement is about 20% over the whole energy interval presented in Fig.2. The maximum values of the enhancement at different collimation are $\mu_{max}(\vartheta_{out} \leq 180^\circ) \simeq 6.09$, $\mu_{max}(\vartheta_{out} \leq 24^\circ) \simeq 5.92$, $\mu_{max}(\vartheta_{out} \leq 12^\circ) \simeq 5.67$, and $\mu_{max}(\vartheta_{out} \leq 1^\circ) \simeq 5.29$. Apparently, they diminish as a collimation angle does so. Shown in Fig.3 is the same as in Fig.2 but for the target thickness $L = 9.0$ mm. The yield at $\vartheta_{out} \leq 1^\circ$ (open circles) is multiplied now by 30. A qualitative behavior of spectra depending on the collimation angle at $L = 9.0$ mm is the same as at $L = 2.2$ mm. However, all the spectra become softer for the larger target thickness. This is indicated already by the increase in $\varepsilon^{(1)}$, $\varepsilon^{(2)}$ values which are now $\varepsilon_{cr}^{(1)} \simeq 85$ MeV, $\varepsilon_{cr}^{(2)} \simeq 185$ MeV, $\varepsilon_{am}^{(1)} \simeq 75$ MeV, $\varepsilon_{am}^{(2)} \simeq 165$ MeV. It is clear that the magnitude of the yield from the thicker target is essentially larger but this increase is different in the crystal and amorphous cases. For example, in the energy range $\varepsilon < 45$ MeV the yield is increased by $6 \div 7$ times for a crystal and by $17 \div 20$ times for amorphous samples. As a result, the enhancement at $L = 9.0$ mm is almost 3 times less than at $L = 2.2$ mm in this energy range. At $L = 9.0$ mm the enhancement is peaked in the first bin ($\varepsilon \in (5 \div 15)$ MeV) for every collimation. Its maximum values are $\mu_{max}(\vartheta_{out} \leq 180^\circ) \simeq 2.25$, $\mu_{max}(\vartheta_{out} \leq 24^\circ) \simeq 2.15$, $\mu_{max}(\vartheta_{out} \leq 12^\circ) \simeq 2.08$, and $\mu_{max}(\vartheta_{out} \leq 1^\circ) \simeq 2.06$. The enhancement monotonically decreases with growing positron energy and approximately halves at $\varepsilon \approx 250$ MeV. Thus, positron spectra from a crystal target are softer at $L = 9.0$ mm as well, and this property is much more pronounced in comparison with $L = 2.2$ mm.

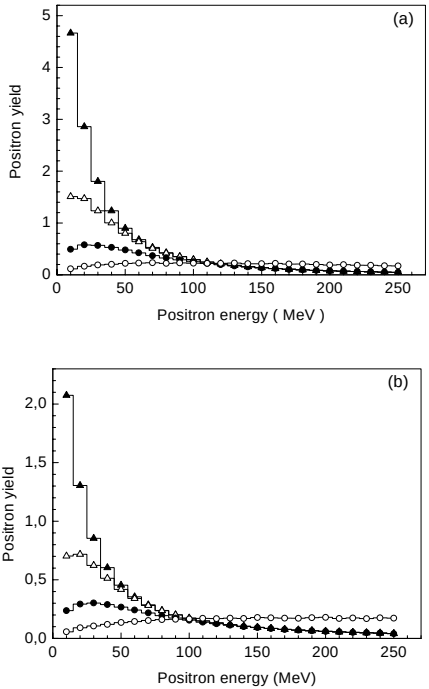

Figure 3: Positron yield depending on energy from 9.0-mm-thick crystal (a) and amorphous (b) targets at different collimation. Filled triangles - no collimation ($\vartheta_{out} \leq 180°$), open triangles - $\vartheta_{out} \leq 24°$, filled circles - $\vartheta_{out} \leq 12°$, and open circles - $\vartheta_{out} \leq 1°$ (multiplied by 30).

Matching systems can be characterized also by a maximum transverse momentum $p_{\perp}^{max}$ of accepted positrons. In this connection, spectra of positrons having $p_{\perp} < p_{\perp}^{max}$ are of undoubted interest. Such spectra at $L = 2.2$ mm (a) and at $L = 9.0$ mm (b) from crystal and amorphous targets are shown in Fig.4 In contrast to the case of the pure angular selection (cf. Figs.2,3), the position of spectral maxima at limited $p_{\perp}$ values is always in the first bin ($\varepsilon \in (7.5 \div 12.5)$ MeV). Corresponding maximum values are $\mu_{max}(5\ MeV/c) \simeq 5.82$, $\mu_{max}(2.5\ MeV/c) \simeq 5.62$ at $L = 2.2$ mm and $\mu_{max}(5\ MeV/c) \simeq 2.17$, $\mu_{max}(2.5\ MeV/c) \simeq 2.11$ at $L = 9.0$ mm. The enhancement monotonically decreases with growing positron energy. Its

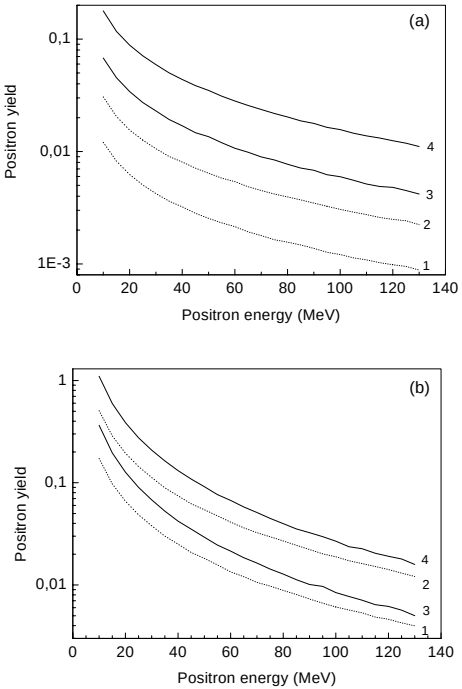

Figure 4: Positron yield depending on energy at $L = 2.2$ mm (a) and $L = 9.0$ mm (b) for $p_{\perp}^{max} = 2.5$ MeV/c (curves 1 and 3) and for $p_{\perp}^{max} = 5$ MeV/c (curves 2 and 4). Solid curves represent the yield from crystal and dotted from amorphous targets.

variation over the whole energy interval presented in Fig.4 is about 15% at $L = 2.2$ mm and 40% at $L = 9.0$ mm. So, for this selection too, positron spectra from crystal targets are softer than those from amorphous targets of the same thickness. The interesting feature of spectral curves in Fig.4 is the similarity of those obtained for two different values of $p_{\perp}^{max}$ from the same target. The scaling factors η are $\eta_{cr} \simeq 2.6$, $\eta_{am} \simeq 2.5$ at $L = 2.2$ mm and $\eta_{cr} \simeq 3.1$, $\eta_{am} \simeq 3.0$ at $L = 9.0$ mm. These factors turn out to be practically (within an accuracy of a few percent) independent of the total positron momentum p. This fact can be easily understood if we assume that a width of the angular distribution of positrons is completely due to multiple scattering

being, thereby, proportional to p^{-1}. Such assumption is confirmed by results of the calculation shown in Fig.5 for two groups of positrons. One of them contains positrons having momentum in the interval $p \in (8.5 \div 11.5)$ Mev/c, for another group $p \in (17 \div 23)$ Mev/c. For a given target, a width of the

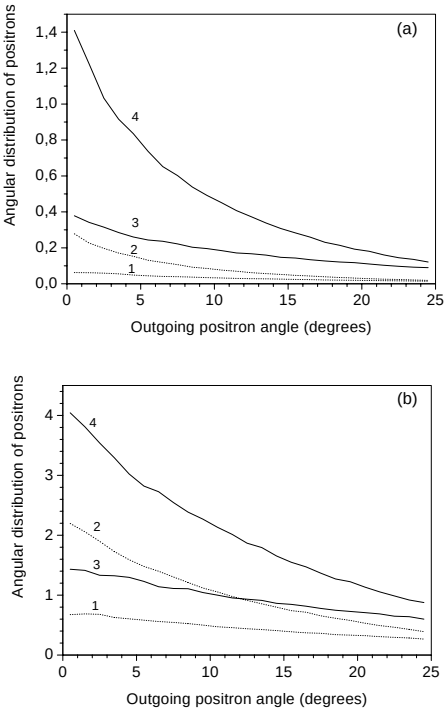

Figure 5: Angular distribution $dN^{(+)}/d\Omega$ depending on outgoing positron angle at $L = 2.2$ mm (a) and at $L = 9.0$ mm (b) for $p \in (8.5 \div 11.5)$ Mev/c (curves 1 and 3) and for $p \in (17 \div 23)$ Mev/c (curves 2 and 4). Solid curves represent the yield from crystal and dotted from amorphous targets.

angular distribution of positrons with $p \approx 10$ Mev/c is approximately twice as much that for $p \approx 20$ Mev/c as expected. The width of every distribution evidently increases when we go on to the thicker target of the same kind. Comparing angular distributions from crystal and amorphous targets of the same thickness, we find that at $L = 9.0$ mm the distributions are somewhat (about 1.5°) wider in the crystal case for both groups. In units of FWHM of

the distribution from the crystal target these differences are about 6.5% at $p \approx 10$ Mev/c and 14% at $p \approx 20$ Mev/c. At $L = 2.2$ mm the distribution from the crystal target is wider by 15.5% at $p \approx 20$ Mev/c whereas this is narrower by 10% at $p \approx 10$ Mev/c.

Going on to a comparison of our results with those obtained in [15], let us remind that to perform an accurate comparison of such kind, exact information is needed concerning the acceptance conditions and registration efficiency of detectors in the experiment. As noted in [15], at $p = 20$ Mev/c, the momentum acceptance ($\Delta p/p$) was 3% (FWHM) and the polar angle acceptance was less than 20 mrad (FWHM). Since the shape of the acceptance curves was unavailable to us, we have tried to simulate experimental conditions using the same angular collimation $\vartheta_{out} \leq \vartheta_{out}^{max}$ and the same value of $\Delta p/p$ for all momenta and targets. So, at the calculation of the magnitudes of positron production efficiency (PPE), we simply put ϑ_{out}^{max} to 20 mrad. The value of $\Delta p/p$ was chosen to reproduce at applied collimation the experimental magnitude of PPE for the 9.0-mm-thick amorphous target. Acting in this way, we have got $\Delta p/p = 3.2\%$. We realize that our regard for the acceptance conditions is rather rough. An additional inaccuracy was introduced when we determined the PPE numbers from Fig.5 of [15]. Note that the experimental numbers obtained in such a way, which are presented by filled symbols in Fig.6, do not reproduce exactly the whole set of mean experimental values for the enhancement given in Table 1 of [15]. Moreover, in Fig.5 of [15] there are no experimental points for 2.2 and 5.3-mm-thick amorphous targets. In these cases the values of PPE given by smooth-curve fits presented in Fig.5 of [15] were used by us as experimental results. Bearing all this in mind, we, nevertheless, can assert that a rather good agreement is seen in Fig.6 of the experimental results and our estimations. Relative difference of them is better than 13% everywhere except the values of PPE at $p = 10$ and 15 Mev/c from both thinnest ($L = 2.2$ mm) targets, where the experimental yield is underestimated by 19% to 42%. Note that just for this thickness the largest inaccuracy was introduced while determining the PPE numbers from Fig.5 of [15] at $p = 10$ and 15 Mev/c, as the magnitude of the yield is especially small in this case.

In contrast to the magnitude of the positron yield, the enhancement is not very sensitive to the acceptance conditions. The calculated values of the enhancement(theory) are presented in Table 1 along with those taken from Table 1 of [15] (experiment). Purely statistical errors are figured in Table 1 as theoretical ones. The relative error in PPE was estimated as $N_{ef}^{-1/2}$, where N_{ef} is the mean number of events in the phase space corresponding

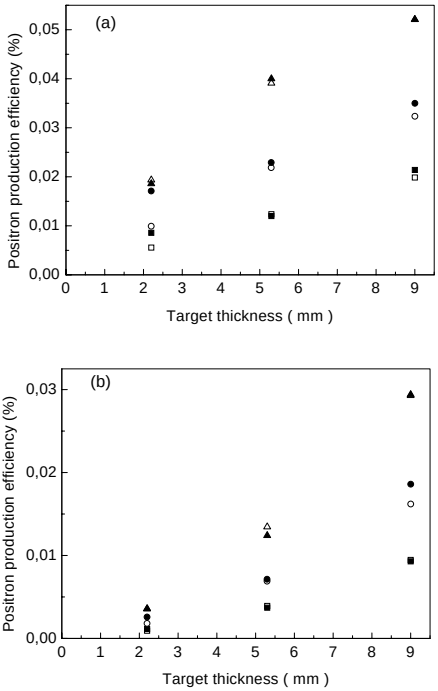

Figure 6: Positron production efficiency from crystal (a) and amorphous (b) targets depending on thickness. Open symbols - our calculation, filled symbols - results from Fig.5 of [15]; $\triangle$ are for $p = 20$ Mev/c, $\bigcirc$ are for $p = 15$ Mev/c, and $\square$ are for $p = 10$ Mev/c.

to the acceptance conditions used in calculations. The total statistics was chosen so that approximately to equalize values of N_{ef} for amorphous and crystal targets of the same thickness. At given total statistics, the quantity N_{ef} increases with growing positron momentum in accord with a shape of the positron spectra at hard collimation shown in Figs.2,3. This fact leads to a better statistical accuracy for larger momentum. We emphasize that the differences of the estimated and experimental enhancement values are smaller than corresponding experimental errors for all momenta and samples figured in Table 1.

Table 1: Enhancement of the positron yield from crystal targets

Momentum (MeV/c)	Enhancement (2.2-mm-thick)		Enhancement (5.3-mm-thick)		Enhancement (9.0-mm-thick)	
	theory	experiment	theory	experiment	theory	experiment
10	6.0 ± 0.5	6.5 ± 0.6	3.2 ± 0.3	3.4 ± 0.7	2.1 ± 0.2	2.3 ± 0.4
15	5.5 ± 0.3	6.2 ± 0.8	3.2 ± 0.2	3.2 ± 0.5	2.0 ± 0.1	2.0 ± 0.2
20	5.4 ± 0.2	5.1 ± 0.5	2.9 ± 0.1	3.0 ± 0.5	1.8 ± 0.1	1.8 ± 0.2

3 Conclusion

Using a simple computer code suggested in [11] and [10], we have compared the theoretical predictions for some characteristics of the electromagnetic shower developing in axially aligned crystals with experimental results reported in [12],[13] and [14],[15]. On the whole, theory and experiment are consistent within an experimental accuracy. From this comparison we also conclude that the accuracy provided by the existing simplified code is at least better than 20%. This accuracy may be slightly improved if we include into consideration some processes like annihilation of positrons or Compton scattering of photons which were ignored as corresponding cross sections are small in the energy region of interest. However, the approximate character of the radiation spectra at axial alignment used in our calculations still provides the main theoretical uncertainty. Nevertheless, we believe that a level of the accuracy already achieved in the theoretical description is quite sufficient to make a reliable choice for optimal parameters of the positron source using axially aligned single crystals.

Acknowledgements

We are grateful to Prof. H.Okuno for providing us with details of the experiment [15] and to the authors of [13] for numerous fruitful discussions. Support of this work by the Russian Fund of Basic Research under Grants 00-02-18007, 01-02-16926, and 01-02-22003 is also gratefully acknowledged.

References

[1] *V.N.Baier, V.M.Katkov and V.M.Strakhovenko.* Phys. stat. sol. (b) **133** (1986) 583.

[2] *V.N.Baier and R.Chehab.* Positron Source based on Channeling Radiation, Proposal for an Experiment at Orsay, LAL, Orsay, France (May 1990).

[3] *V.N.Baier, V.M.Katkov and V.M.Strakhovenko.* Sov. Phys. Usp. **32** (1989) 972.

[4] *V.N.Baier, V.M.Katkov and V.M.Strakhovenko.* Electromagnetic Processes at High Energies in Oriented Single Crystals, World Scientific Publishing Co, Singapore, 1998.

[5] *V.N.Baier, V.M.Katkov and V.M.Strakhovenko.* Nucl. Instr. and Meth. A **250** (1986) 514.

[6] *V.N.Baier, V.M.Katkov and V.M.Strakhovenko.* Nucl. Instr. and Meth. B **27** (1987) 360.

[7] *R.Medenwaldt et al.* Phys. Lett. B **227** (1989) 483.

[8] *V.N.Baier, V.M.Katkov and V.M.Strakhovenko.* Nucl. Instr. and Meth. B **119** (1996) 131.

[9] *V.N.Baier, V.M.Katkov and V.M.Strakhovenko.* Phys. stat. sol.(b) **149** (1988) 403.

[10] *V.N.Baier and V.M.Strakhovenko.* Nucl. Instr. and Meth. B **155** (1999) 403.

[11] *V.N.Baier, V.M.Katkov and V.M.Strakhovenko.* Nucl. Instr. and Meth. B **103** (1995) 147.

[12] *R.Chehab et al.* Proceedings of LINAC2000, Monterey, CA, USA, August 2000, p.143

[13] *R.Chehab et al.* Report on RREPS-01 Conference, Lake Aya, Russia, September 2001.

[14] *M.Inoue, S.Takenaka, K.Yoshida et al.* Nucl. Instr. and Meth. B **173** (2001) 104.

[15] *H.Okuno et al.* Report on RREPS-01 Conference, Lake Aya, Russia, September 2001; KEK Preprint 2001-146.

V.N. Baier and V.M. Strakhovenko

Comparison of theory with experiment for positron production from high-energy electrons moving along crystal axes

Budker INP 2002-14

Ответственный за выпуск А.М. Кудрявцев
Работа поступила 27.02.2002 г.

Сдано в набор 4.03.2002 г.
Подписано в печать 6.03.2002 г.
Формат бумаги 60×90 1/16 Объем 0.9 печ.л., 0.8 уч.-изд.л.
Тираж 125 экз. Бесплатно. Заказ № 14

Обработано на IBM PC и отпечатано на
ротапринте ИЯФ им. Г.И. Будкера СО РАН
Новосибирск, 630090, пр. академика Лаврентьева, 11.